Eur J Nucl Med Mol Imaging (2013) 40:356–363
DOI 10.1007/s00259-012-2278-6

ORIGINAL ARTICLE

The diagnostic value of ^{18}F-FDG PET and MRI in paediatric histiocytosis

Wolfgang Peter Mueller · Henriette Ingrid Melzer · Irene Schmid · Eva Coppenrath · Peter Bartenstein · Thomas Pfluger

Received: 21 August 2012 / Accepted: 4 October 2012 / Published online: 25 October 2012

Abstract
Purpose To analyse the diagnostic value of ^{18}F-FDG PET and MRI for the evaluation of active lesions in paediatric Langerhans cell histiocytosis.
Methods We compared 21 ^{18}F-FDG PET scans with 21 MRI scans (mean time interval 17 days) in 15 patients (11 male, 4 female, age range 4 months to 19 years) with biopsy-proven histiocytosis. Primary criteria for the lesion-based analysis were signs of vital histiocyte infiltrates (bone marrow oedema and contrast enhancement for MRI; SUV greater than the mean SUV of the right liver lobe for PET). PET and MR images were analysed separately and side-by-side. The results were validated by biopsy or follow-up scans after more than 6 months.
Results Of 53 lesions evaluated, 13 were confirmed by histology and 40 on follow-up investigations. The sensitivity and specificity of PET were 67 % and 76 % and of MRI were 81 % and 47 %, respectively. MRI showed seven false-positive bone lesions after successful chemotherapy. PET showed five false-negative small bone lesions, one false-negative lesion of the skull and three false-negative findings for intracerebral involvement. PET showed one false-positive lesion in the lymphoid tissue of the head and neck region and two false-positive bone lesions after treatment. Combined PET/MR analysis decreased the number of false-negative findings on primary staging, whereas no advantage over PET alone was seen in terms of false-positive or false-negative results on follow-up.
Conclusion Our retrospective analysis suggests a pivotal role of ^{18}F-FDG PET in lesion follow-up due to a lower number of false-positive findings after chemotherapy. MRI showed a higher sensitivity and is indispensable for primary staging, evaluation of brain involvement and biopsy planning. Combined MRI/PET analysis improved sensitivity by decreasing the false-negative rate during primary staging indicating a future role of simultaneous whole-body PET/MRI for primary investigation of paediatric histiocytosis.

Keywords PET/MRI · MR/PET · Histiocytosis · Paediatric oncology

W. P. Mueller (✉) · H. I. Melzer · P. Bartenstein · T. Pfluger
Department of Nuclear Medicine,
Ludwig-Maximilians-University of Munich,
Marchioninistraße 15,
81377 Munich, Germany
e-mail: wolfgang.mueller@med.uni-muenchen.de

I. Schmid
Department of Paediatric Oncology,
Ludwig-Maximilians-University of Munich,
Munich, Germany

E. Coppenrath
Department of Radiology,
Ludwig-Maximilians-University of Munich,
Munich, Germany

Introduction

Langerhans cell histiocytosis (LCH) refers to a group of disorders involving clonal proliferation of activated dendritic cells and macrophages. LCH usually affects children between the ages of 1 and 15 years and is traditionally divided by number of lesions and lesion distribution into three groups: (1) unifocal eosinophilic granuloma, which is predominantly osseous or pulmonary; (2) single-system multifocal, e.g. multifocal bone lesions; and (3) multifocal multisystem, e.g. Abt-Letterer-Siwe disease, which typically includes the abdominal viscera [1]. Typically involved are bone, lung, skin and lymph nodes, but during the course of the disease any organ system may be affected [2]. Prognosis is determined by the involvement of organs at risk (liver, spleen, haematopoietic system) and response to treatment which makes cross-sectional whole-body imaging the first choice for evaluation of active disease [3, 4].

PET and MRI have been proven to reliably identify multifocal disease [5]. PET has been shown to locate primary LCH lesions with high accuracy and provides important information on follow-up as decreased ^{18}F-FDG uptake can be seen after successful chemotherapy [6, 7]. MRI has become an integral part of LCH staging [8]. Perilesional oedema detected as signal hyperintensity on T2-weighted images and contrast enhancement are used as hallmarks of lesion activity. Previous reports have underlined the value of MRI for detecting skeletal as well as intracerebral involvement [9–11]. Image acquisition with high spatial resolution and good soft-tissue contrast further enables biopsy planning in complex anatomic sites.

The first integrated whole-body PET/MRI scanners have been introduced into clinical practice and research. Paediatric tumour entities that require both PET and MR imaging may be more adequately evaluated by combined PET/MRI. The aim of this retrospective study was to compare the diagnostic value of ^{18}F-FDG PET with that of MRI in primary staging and follow-up of paediatric LCH lesions. We also review the future prospects for the use of combined PET/MRI devices for this purpose.

Materials and methods

Search algorithm

Whole-body MRI and ^{18}F-FDG PET were performed in patients with suspected LCH for primary staging or at least 6 weeks after chemotherapy for follow-up. ^{18}F-FDG PET and MRI scans in 15 patients with a maximum of 30 days and no tumour-specific treatment between single investigations were compared. CT scans were taken for comparison only if pulmonary involvement was suspected and were not included in the study. In summary, 53 lesions from 15 patients were evaluated, of which 25 were evaluated for primary staging and 28 for follow-up after chemotherapy. Six lesions evaluated for primary staging were reevaluated after treatment. The mean time between investigations was 17 days.

Patients

Scans were performed in 15 consecutive LCH patients (11 males, 4 females; age range 4 months to 19 years). Patients were referred to the children's hospital for suspected histiocytosis from other hospitals or from private practitioners between January 2006 and March 2011. Written informed consent was available in all patients. All patients had histologically proven histiocytosis. Seven were diagnosed with multifocal LCH and six with unifocal eosinophilic granuloma. One patient showed sinus histiocytosis with massive lymphadenopathy and Rosai-Dorfman disease was diagnosed. In one patient cutaneous LCH was diagnosed. Six lesions in one patient were reevaluated after treatment. The characteristics of the patient population are shown in Table 1.

Acquisition protocol

Whole-body ^{18}F-FDG PET scans were performed using a Philips Allegro PET scanner (15 scans; Philips Healthcare, Best, The Netherlands) or a GE Discovery 690 PET/CT scanner (six scans; General Electric Company, Fairfield, CT). Whole-body, non-enhanced, low-dose CT (10 mA, 140 kV) or transmission scans with a ^{137}Cs source were used for attenuation correction. Images were acquired in 3-D mode using a row action maximum likelihood algorithm (3-D RAMLA). Patients fasted for at least 6 h and blood glucose levels were determined to exclude hyperglycaemia before ^{18}F-FDG was injected at a dose according to EANM guidelines [12]. Concomitantly with intravenous tracer injection, furosemide in amounts adjusted for body weight were administered to decrease physiological activity in the urinary bladder and to reduce radiation exposure. Patients were kept warm and were instructed to rest until the beginning of the examination. Whole-body PET scans were performed 60 min after administration of ^{18}F-FDG.

MRI scans were performed using a Siemens Magnetom Vision 1.5 T scanner (Siemens, Erlangen, Germany). A set of sequences consisting of short tau inversion recovery (STIR) T2-weighted and T1-weighted turbo spin echo (TSE) sequences before and after administration of gadolinium-DTPA (Magnevist, Schering, Berlin, Germany) at 0.1 mmol/kg body weight were performed in coronal, sagittal or axial orientation including the region of interest or the whole body. The protocol for suspected intracerebral involvement included T2-weighted TSE, T1-weighted TSE before and after administration of contrast agent and T2-weighted fluid attenuated inversion recovery weighted sequences in axial or sagittal orientation.

Image analysis

Retrospective lesion-based image analysis was performed. A lesion was included in the analysis if it was considered positive for active histiocytosis by PET and/or MRI at any point during the course of the disease. The individual PET and MRI scans were analysed by two independent observers with long experience with paediatric PET and MRI studies (T.P. and E.C.). Images were analysed with knowledge of the clinical data. Observers knew the findings from the previous examination with the same modality when necessary in order to evaluate regression or disappearance of lesions.^{18}F-FDG PET images were reviewed on a HERMES workstation (Nuclear Diagnostics, Haegersten, Sweden). MR images were reviewed on a Siemens Syngo PACS system (Siemens, Erlangen, Germany).

Each lesion was judged either positive or negative with regard to vital histiocyte infiltration. On ^{18}F-FDG PET images, a lesion was judged positive if it showed

Table 1 Patient characteristics, number of lesions, biopsies and time points for PET/MRI analysis

Patient no.	Gender	Age (years/months)	Clinical diagnosis	No. of biopsy-proven lesions for PET/MR analysis	Total no. of biopsy-proven lesions	Prior therapy	No. of lesions for PET/MR analysis	Total no. of lesions	System involvement	No. of time points for PET/MRI
1	M	7/1	EG	1	1	None	1	1	Unifocal	1
2	F	5/5	EG	1	1	None	1	1	Unifocal	1
3	M	14/5	EG	1	1	None	1	1	Unifocal	1
4	M	19/3	EG	1	1	None	1	1	Unifocal	1
5	F	2/5	EG	1	1	None	1	1	Unifocal	1
6	M	10/11	EG	1	1	Chemotherapy	1	1	Unifocal	1
7	M	0/5	CL	0	1	None	1	1	Single-system multifocal	1
8	M	8/4	RD	4	4	Chemotherapy	5	5	Multisystem	1
9	M	15/3	LCH	1	1	None	3	3	Multisystem	1
10	F	7/2	LCH	0	1	None	14	8	Multisystem	2
11	M	10/5	LCH	1	1	None	1	4	Multisystem	1
12	F	0/8	LCH	1	1	None	7	8	Multisystem	1
13	M	11/4	LCH	0	1	Chemotherapy	6	7	Single-system multifocal	2
14	M	15/5	LCH	0	1	Chemotherapy	5	5	Single-system multifocal	1
15	M	6/9	LCH	0	1	Chemotherapy	5	8	Multisystem	1

CL cutaneous LCH, *EG* eosinophilic granuloma, *LCH* Langerhans cell histiocytosis, *RD* Rosai-Dorfman disease.

nonphysiological ^{18}F-FDG uptake that was higher than the mean uptake of the patient's right liver lobe. On the MRI scans, a lesion was judged positive depending on size, shape and contrast enhancement on T1-weighted images, and perilesional oedema on T2-weighted images. A diagnostic confidence score was assigned to each lesion as follows: *1* unsure, *2* suspected, *3* certain. For combined analysis PET and MRI were reviewed side-by-side on one workstation. In case of discrepant findings the finding of the modality with the higher diagnostic confidence score was used. If both modalities revealed the same confidence score the lesion was judged positive.

Standard of reference

The standard of reference was histopathology (13 lesions) or evaluation by follow-up scans (40 lesions). For verification, PET or MRI follow-up examinations were evaluated after a minimum of 6 months after the primary investigations. A lesion was classified either "false-positive" or "true-negative" if it disappeared without any tumour-specific therapy during the observation period, or if it turned out to be an obvious physiological structure or uptake. A nonphysiological structure was classified either "true-positive" or "false-negative" if it persisted or progressed during follow-up, or showed an objective regression under specific therapy.

Results

Of 53 lesions evaluated, 36 were proven to be active histiocytosis by histology or follow-up imaging. The majority of lesions were localized in the skeleton. Five suspected infiltrates were seen for lymph nodes in the head and neck region. Three intracerebral lesions and two suspected pulmonary lesions were evaluated. Five suspected lesions of the ear/nose/throat mucosa and one thymic involvement were seen. Anatomical lesion sites and numbers of lesions are shown in Table 2.

Table 2 Anatomical distribution of 53 lesions

Anatomical site of lesion	Number of lesions
Bone	37
Extremities	19
Skull	8
Spine	7
Pelvis	3
Brain	3
Lung	2
Lymph nodes	5
Thymus	1
Ear/nose/throat mucosa	5

^{18}F-FDG PET versus MRI for the evaluation of active lesions

The mean diagnostic confidence score was 2.3 for MRI and 2.2 for ^{18}F-FDG PET. Positive and negative decisions for true and false findings as well as sensitivity and specificity for each modality are shown in Table 3. The sources of the false-positive and false-negative findings are shown in Table 4.

^{18}F-FDG PET showed one false-positive finding in a patient with multifocal histiocytosis most likely due to post-inflammatory uptake in lymphoid tissue of the nasopharynx. Two false-positive results were seen for bone lesions after chemotherapy.

False-negative PET results (12 lesions) were mainly small bone infiltrates (five lesions, mean largest diameter 12 mm; Fig. 1a, b) and lymphoid tissue and mucosa of the head and neck region (three lesions). All small bone lesions were correctly identified by their hyperintense pattern on the corresponding T2-weighted STIR MR images, whereas infiltrates of the head and neck region were also missed by MRI. Four intracerebral and cranial lesions were false-negative on PET most likely due to high physiological uptake in the adjacent cerebral cortex (Fig. 1c, d). Intracerebral and cranial lesions were clearly identified by MRI.

On MRI analysis, there were seven false-positive findings for suspected bone lesions in five individual patients after successful chemotherapy: two lesions of the vertebral column and in five lesions of the extremities. During primary and follow-up investigations, lesions showed contrast enhancement on T1-weighted images or signs of bone marrow oedema on T2-weighted images, whereas they remained ^{18}F-FDG-negative on PET (Fig. 2). One false-positive MRI finding was seen in a patient with contrast enhancement and oedema of the middle ear that was most likely due to otitis. Two small vertebral infiltrates, two cervical lymph nodes, two sinus infiltrates and two cases of intrapulmonary involvement were false-negative on MRI. Three out of three cases of intracerebral involvement were correctly identified on MRI as white matter lesions or infundibular enlargement on T1-weighted and T2-weighted images (Fig. 1b, c).

In two cases hypermetabolic intrapulmonary lesions were seen on PET images and were judged as intrapulmonary histiocyte infiltrates. Inspiratory high-resolution CT images were available (mean 8 days to MRI/PET). In one patient pulmonary histiocytosis was confirmed by CT. CT images of the other patient showed a bronchiogenic cyst without evidence of pulmonary histiocytosis. MR images of the thorax revealed no abnormal findings in either patient.

Table 3 PET versus MR imaging findings in 53 lesions

	MRI	PET
True-positive findings	29	24
True-negative findings	8	13
False-positive findings	9	4
False-negative findings	7	12
Sensitivity (%)	81	67
Specificity (%)	47	76

Primary staging versus follow-up after treatment

In order to determine the additional value of combined imaging for primary staging or follow-up, lesions were divided into two groups: lesions that were detected during primary staging (n=25) and lesions that were evaluated on follow-up (n=28). The numbers of false-positive and false-negative results for each modality as well as for the combined analysis of both groups are shown in Table 5.

On primary staging, PET showed a higher rate of false-negative findings than MRI (seven versus one). In the combined MRI/PET analysis, the higher confidence score with MRI for small bone infiltrates and brain lesions decreased the number of false-negative decisions. In one case, PET corrected a false-negative MRI finding of a cervical lymph node in a patient with multifocal Langerhans disease.

On posttreatment follow-up, MRI analysis showed a higher rate of false-positive decisions especially for bone lesions. Comparable rates of false-negative findings were seen for PET and MRI. In the combined analysis, false MRI decisions relating to larger residual bone marrow oedema after chemotherapy were corrected by PET. However, smaller residual changes remained false-positive in the combined MRI/PET analysis because of a higher confidence score of MRI for small bone lesions.

Discussion

^{18}F-FDG PET

The use of ^{18}F-FDG PET for the evaluation of paediatric LCH is well established. Previous studies have shown high sensitivity and specificity of ^{18}F-FDG PET, which was superior to bone scans and conventional radiography for overall lesion detection [6, 13, 14]. In addition, PET is excellent for lesion follow-up after chemotherapy and provides information on response earlier than plain film radiography or CT [7, 13–15].

Our study confirmed an overall high sensitivity of PET, which was however lower than that of MRI. The majority of false-negative PET results were seen for small bone

Table 4 Sources of false PET/MRI findings

Modality	Finding	Source
MRI	False-positive	Posttherapy bone marrow oedema/contrast enhancement (n=7); otitis (n=1); physiological structure (n=1)
	False-negative	Small bone lesion (n=2); no abnormality in ear/nose/throat mucosa (n=2), lymph nodes (n=2), lungs (n=1)
PET	False-positive	Inflammation (n=1); posttherapy bone marrow uptake (n=2); benign bronchiogenic cyst (n=1)
	False-negative	Small bone lesion (n=5); physiological uptake in ear/nose/throat mucosa/lymph nodes (n=3); lesion close to brain (n=4)

infiltrates (mean diameter 12 mm) that are difficult to detect even with modern PET scanners. The higher spatial resolution of MRI than of conventional radiography and its ability to detect even small bone infiltrates may have led to a lower PET sensitivity than previously described by others. However, PET was superior to MRI in terms of specificity, especially for bone lesions after chemotherapy. Glucose metabolism normalized early and remained stable in most bone lesions after treatment. False-positive decisions in the follow-up PET analysis were only made for a hypermetabolic pulmonary cyst and

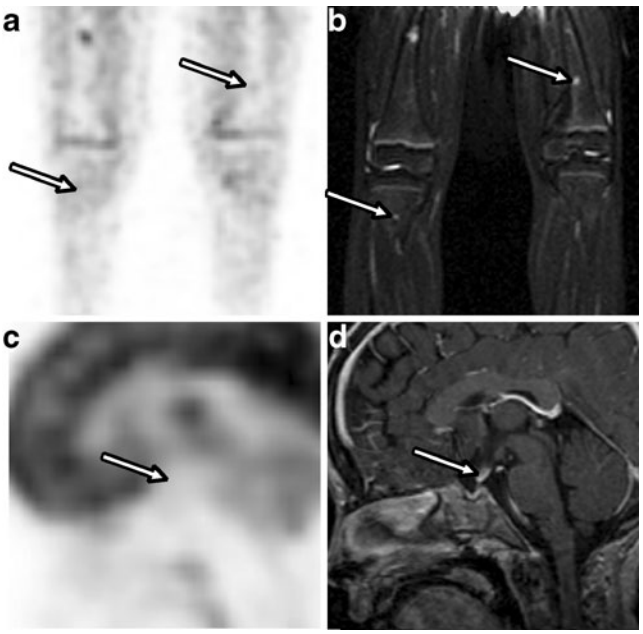

Fig. 1 False-negative PET findings in a 7-year-old girl with diabetes insipidus and multifocal bone lesions. **a**, **b** Small bone lesions. FDG signal decreases with lesion size. Bone infiltration of the right distal femur is seen as a hypermetabolic signal on the coronal PET image (**a**) and as a hyperintense signal on the coronal MRI T2-weighted STIR image (**b**), whereas smaller bone lesions of the left distal femur and the right tibia (*arrows*) show only mild to no increase in FDG uptake. **c**, **d** Intracerebral lesion. Contrast enhancement and thickening of the infundibulum can be seen on the sagittal T1-weighted MR image (**d**, *arrow*), whereas the PET image shows normal findings (**c**). Intracerebral involvement was confirmed by follow-up MRI

for increased ^{18}F-FDG uptake in two bone marrow lesions, and may have been caused by posttherapy tissue remodelling and regeneration. Patients with LCH, especially in the low risk group, show excellent response rates to chemotherapy with prednisone and vinblastine [16]. Treatment response dramatically improves the probability of survival [16]. Therefore, a high specificity of PET is important to avoid false decisions on disease activity and unnecessary treatment, and to improve risk stratification.

LCH lesions in the brainstem and cerebellum can be detected by ^{18}F-FDG PET and follow-up examinations have been shown to be useful for monitoring CNS disease activity [17]. In our study, however, the ^{18}F-FDG uptake of the cerebral cortex and subcortical nuclei most likely interfered with uptake patterns of the intracerebral infiltrates and led to false-negative decisions in three out of three confirmed cases.

In our study pulmonary LCH was correctly identified by PET in only one out of two patients. Small infiltrates may not be detected by a modality with limited spatial resolution under continuous respiratory motion. However, in patients with more advanced nodular pulmonary LCH, increased glucose uptake of the lung parenchyma can been seen on PET scans [18]. In these patients the ratio of lung to liver uptake may be useful to detect and reevaluate disease activity [19].

MRI

MRI detects bone marrow involvement or soft tissue masses in LCH with high sensitivity [6, 9, 20, 21]. Bone lytic lesions are isointense to muscle on T1-weighted MR images. Enhancement on T1-weighted images after administration of gadolinium contrast agent is seen as a correlate of lesion activity or perilesional inflammation [5]. A T2 hyperintense signal in LCH lesions, the surrounding bone marrow, periosteum or soft tissue can be detected as a correlate of oedema [22]. Fast whole-body T2-weighted STIR protocols are used to screen the entire body for bone involvement [23].

Our retrospective analysis confirmed a high sensitivity for bone infiltrates. Only two out of 18 true-positive bone

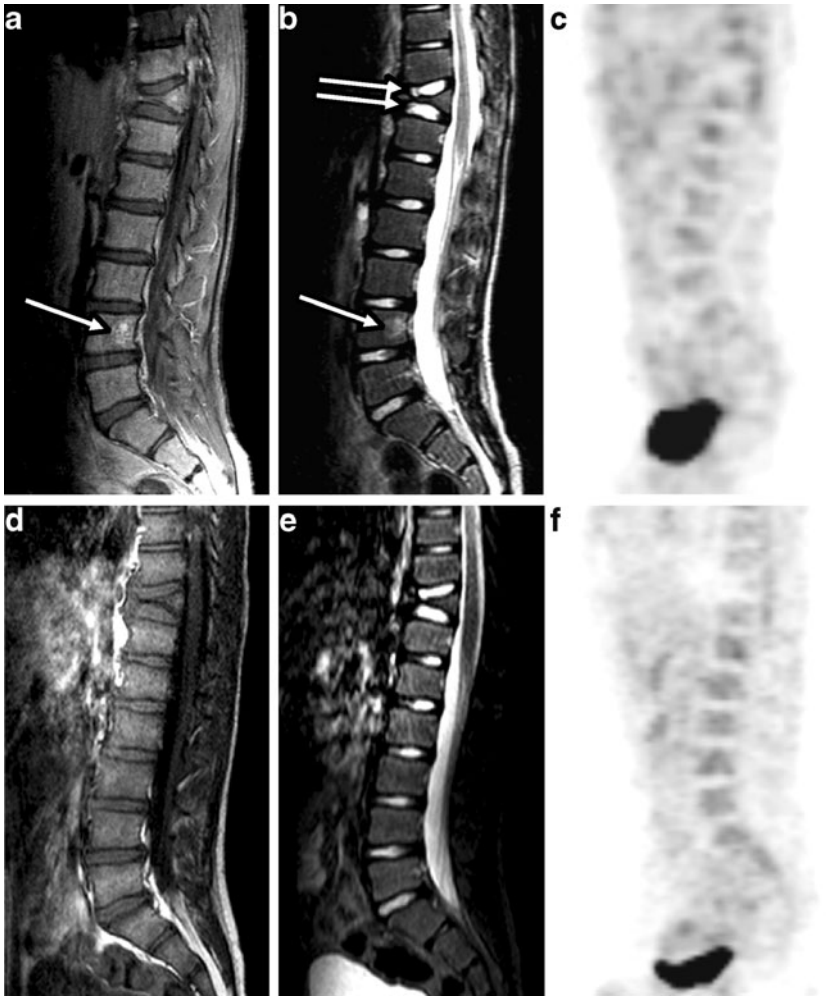

Fig. 2 False-positive MRI findings in a 10-year-old boy with multifocal skeletal involvement. **a–c** Six months after chemotherapy with prednisone and vinblastine. A T2-weighted STIR hyperintense lesion (**b**, *arrow*) with contrast enhancement on the T1-weighted sagittal MR image (**a**, *arrow*) is seen in lumbar vertebra 4, whereas PET shows normal FDG uptake (**c**). In addition a vertebra plana is seen in thoracic vertebra 11 (**b**, *double arrow*). **d–f** Follow-up imaging after 12 months. No contrast-enhancing lesion (**d**) or T2-hyperintense lesion (**e**) is seen on the MR images. The PET image remains negative for metabolic activity (**f**)

lesions were not detected by MRI. However, T2 hyperintensity and contrast enhancement of residual bone marrow lesions could represent false-positive findings potentially leading to incorrect decisions after chemotherapy. Three lesions in two patients showed contrast enhancement and a high T2 signal after chemotherapy. One lesion was located in the spine and two in the femur. In four lesions, a T2 hyperintense signal of the bone marrow resulted in false-positive MRI decisions. In all lesions contrast enhancement and T2 hyperintensity resolved over a period of 12 months even without further treatment. PET was negative for these lesions and remained negative throughout a treatment-free interval. Abnormalities on cranial MR images in patients with intracerebral involvement include asymmetric T2 hyperintense lesions of the cerebellar white matter and the brainstem, and less often hyperintense patterns of the cerebral white matter or the basal ganglia. Intracerebral LCH lesions are often hypointense on T1-weighted images and may show contrast enhancement. Infundibular enlargement may be seen in patients with diabetes insipidus caused by involvement of the hypothalamic-pituitary axis [24].

Table 5 False-positive and false-negative results with PET, MRI and combined MRI/PET in primary staging and follow-up

	Finding	MRI	PET	Combined MRI/PET
Primary staging	False-positive	2	1	1
	False-negative	1	7	0
Follow-up	False-positive	7	3	5
	False-negative	6	5	4

Our study confirmed the importance of MRI for the evaluation of central nervous system disease. In three out of three patients, intracerebral involvement was correctly identified by MRI, whereas PET failed to detect pathological uptake patterns. T2-weighted MRI depicts concomitant diffuse white matter oedema, whereas PET only detects metabolic activity in the lesion itself. Here imaging oedema is more sensitive than imaging glucose metabolism in a body region with strong physiological ^{18}F-FDG uptake.

As with PET, pulmonary involvement was not accurately diagnosed using MRI. Magnetic susceptibility effects of large magnetic field gradients between air and lung tissue, a low signal to noise ratio of the inflated lungs as well as motion artefacts limit evaluation of subtle interstitial changes caused by intrapulmonary infiltrates [25].

Limitations

There were some limitations to our study. The disorder under investigation is rare so this imaging study was based on a limited number of patients. In patients with multifocal histiocytosis, histopathology was mostly obtained only from one lesion in order to confirm the diagnosis. Therefore, even though in all patients LCH was confirmed by biopsy, a smaller percentage of single lesions was confirmed by histology. Multiple follow-up PET and MRI scans were used when available to ensure the validity of judgements on lesion vitality after treatment. Still, the standard of reference should be histology for the majority of lesions to avoid statistical errors.

In our study design, lesions nondetectable by both modalities could not be distinguished from nonexistent lesions. Therefore sensitivity would have been overestimated for both modalities. In addition, our algorithm for combined analysis in which lesions were judged positive if the two modalities were discrepant would have further raised sensitivity and lowered specificity.

Conclusion and future prospects on combined PET/MRI acquisition

In our retrospective study, the diagnostic value of PET was compared with that of MRI in patients with LCH for primary staging and disease follow-up. ^{18}F-FDG PET was more accurate in evaluating disease activity after chemotherapy. Decreased glucose metabolism was seen early, whereas residual contrast enhancement and T2 hyperintensity were detected on MR images in several patients. We conclude that ^{18}F-FDG uptake is a hallmark of active lesions whereas oedema and contrast enhancement may more often be induced by posttherapy tissue reorganization.

The overall sensitivity of MRI was superior to that of PET. Brain involvement, in particular, was more accurately diagnosed by MRI. A high sensitivity for tumour lesions in brain, bone, lymph nodes and internal organs is important especially at primary staging as prognosis and therapeutic decisions critically depend on whether organs at risk or multiple organ systems are involved. MRI further gives anatomic information necessary for biopsy planning without additional radiation exposure.

Combined PET/MRI analysis improved false-negative and false-positive rates in primary staging, whereas no clear advantage over PET alone was seen for disease follow-up. Due to our findings, MRI plus ^{18}F-FDG PET is recommended as the method of choice during primary diagnosis whereas ^{18}F-FDG PET alone is sufficient for disease follow-up. An additional inspiratory diagnostic CT scan should always be considered in patients with suspected pulmonary involvement since in these patients both PET and MRI showed limited sensitivity.

Integrated whole-body PET/MRI scanners have recently been introduced into research and clinical practice. A first study in adult patients with oncological diagnoses showed no limitations of PET/MRI versus PET/CT for lesion detection and quantification [26]. In the future, simultaneous PET/MRI acquisition may become the first choice for initial evaluation of patients with LCH and may be able to reduce examination time, sedation and radiation exposure while maintaining a high diagnostic accuracy.

Conflicts of interest None.

Financial support None.

References

1. Hoover KB, Rosenthal DI, Mankin H. Langerhans cell histiocytosis. Skeletal Radiol. 2007;36:95–104.
2. Grois N, Potschger U, Prosch H, Minkov M, Arico M, Braier J, et al. Risk factors for diabetes insipidus in langerhans cell histiocytosis. Pediatr Blood Cancer. 2006;46:228–33.
3. Minkov M, Grois N, Heitger A, Potschger U, Westermeier T, Gadner H. Response to initial treatment of multisystem Langerhans cell histiocytosis: an important prognostic indicator. Med Pediatr Oncol. 2002;39:581–5.
4. Gadner H, Grois N, Arico M, Broadbent V, Ceci A, Jakobson A, et al. A randomized trial of treatment for multisystem Langerhans' cell histiocytosis. J Pediatr. 2001;138:728–34.
5. Schmidt S, Eich G, Geoffray A, Hanquinet S, Waibel P, Wolf R, et al. Extraosseous langerhans cell histiocytosis in children. Radiographics. 2008;28:707–26.
6. Phillips M, Allen C, Gerson P, McClain K. Comparison of FDG-PET scans to conventional radiography and bone scans in management of Langerhans cell histiocytosis. Pediatr Blood Cancer. 2009;52:97–101.
7. Binkovitz LA, Olshefski RS, Adler BH. Coincidence FDG-PET in the evaluation of Langerhans' cell histiocytosis: preliminary findings. Pediatr Radiol. 2003;33:598–602.
8. Meyer JS, De Camargo B. The role of radiology in the diagnosis and follow-up of Langerhans cell histiocytosis. Hematol Oncol Clin North Am. 1998;12:307–26.
9. Azouz EM, Saigal G, Rodriguez MM, Podda A. Langerhans' cell histiocytosis: pathology, imaging and treatment of skeletal involvement. Pediatr Radiol. 2005;35:103–15.
10. Pavlik M, Bloom DA, Ozgonenel B, Sarnaik SA. Defining the role of magnetic resonance imaging in unifocal bone lesions of langerhans cell histiocytosis. J Pediatr Hematol Oncol. 2005;27:432–5.

11. Grois N, Fahrner B, Arceci RJ, Henter JI, McClain K, Lassmann H, et al. Central nervous system disease in Langerhans cell histiocytosis. J Pediatr. 2010;156:873–81.
12. Bombardieri E, Aktolun C, Baum RP, Bishof-Delaloye A, Buscombe J, Chatal JF, et al. FDG-PET: procedure guidelines for tumour imaging. Eur J Nucl Med Mol Imaging. 2003;30:BP115–24.
13. Kaste SC, Rodriguez-Galindo C, McCarville ME, Shulkin BL. PET-CT in pediatric Langerhans cell histiocytosis. Pediatr Radiol. 2007;37:615–22.
14. Blum R, Seymour JF, Hicks RJ. Role of 18FDG-positron emission tomography scanning in the management of histiocytosis. Leuk Lymphoma. 2002;43:2155–7.
15. Lee HJ, Ahn BC, Lee SW, Lee J. The usefulness of F-18 fluorodeoxyglucose positron emission tomography/computed tomography in patients with Langerhans cell histiocytosis. Ann Nucl Med. 2012. doi:10.1007/s12149-012-0635-y
16. Gadner H, Grois N, Potschger U, Minkov M, Arico M, Braier J, et al. Improved outcome in multisystem Langerhans cell histiocytosis is associated with therapy intensification. Blood. 2008;111:2556–62.
17. Buchler T, Cervinek L, Belohlavek O, Kantorova I, Mechl M, Nebesky T, et al. Langerhans cell histiocytosis with central nervous system involvement: follow-up by FDG-PET during treatment with cladribine. Pediatr Blood Cancer. 2005;44:286–8.
18. Krajicek BJ, Ryu JH, Hartman TE, Lowe VJ, Vassallo R. Abnormal fluorodeoxyglucose PET in pulmonary Langerhans cell histiocytosis. Chest. 2009;135:1542–9.
19. Szturz P, Rehak Z, Koukalova R, Adam Z, Krejci M, Pour L, et al. Measuring diffuse metabolic activity on FDG-PET/CT: new method for evaluating Langerhans cell histiocytosis activity in pulmonary parenchyma. Nucl Med Biol. 2012;39:429–36.
20. Mentzel HJ, Kentouche K, Sauner D, Fleischmann C, Vogt S, Gottschild D, et al. Comparison of whole-body STIR-MRI and 99mTc-methylene-diphosphonate scintigraphy in children with suspected multifocal bone lesions. Eur Radiol. 2004;14:2297–302.
21. Goo HW, Yang DH, Ra YS, Song JS, Im HJ, Seo JJ, et al. Whole-body MRI of Langerhans cell histiocytosis: comparison with radiography and bone scintigraphy. Pediatr Radiol. 2006;36:1019–31.
22. Kilborn TN, Teh J, Goodman TR. Paediatric manifestations of Langerhans cell histiocytosis: a review of the clinical and radiological findings. Clin Radiol. 2003;58:269–78.
23. Kellenberger CJ, Epelman M, Miller SF, Babyn PS. Fast STIR whole-body MR imaging in children. Radiographics. 2004;24:1317–30.
24. Grois N, Tsunematsu Y, Barkovich AJ, Favara BE. Central nervous system disease in Langerhans cell histiocytosis. Br J Cancer Suppl. 1994;23:S24–8.
25. Ohno Y, Koyama H, Yoshikawa T, Nishio M, Matsumoto S, Iwasawa T, et al. Pulmonary magnetic resonance imaging for airway diseases. J Thorac Imaging. 2011;26:301–16.
26. Drzezga A, Souvatzoglou M, Eiber M, Beer AJ, Furst S, Martinez-Moller A, et al. First clinical experience with integrated whole-body PET/MR: comparison to PET/CT in patients with oncologic diagnoses. J Nucl Med. 2012;53:845–55.